Power waves and scattering parameters in magneto-inductive systems

A. Voronov, O. Sydoruk, and R. R. A. Syms

COLLECTIONS

F   This paper was selected as Featured

View Online   Export Citation   CrossMark

ARTICLES YOU MAY BE INTERESTED IN

Observations of a plectonemic configuration in a stable magnetized plasma jet
Physics of Plasmas **28**, 040703 (2021); https://doi.org/10.1063/5.0044034

A tri-band mode conversion system for high-power microwave applications
AIP Advances **11**, 045318 (2021); https://doi.org/10.1063/5.0049578

Integration of magnetic tweezers and traction force microscopy for the exploration of matrix rheology and keratinocyte mechanobiology: Model force- and displacement-controlled experiments
AIP Advances **11**, 045216 (2021); https://doi.org/10.1063/5.0041262

Call For Papers!

AIP Advances

SPECIAL TOPIC: Advances in Low Dimensional and 2D Materials

Power waves and scattering parameters in magneto-inductive systems Ⓕ

A. Voronov, ⒾⒹ O. Sydoruk, ⒾⒹ and R. R. A. Syms[a)] ⒾⒹ

AFFILIATIONS

Optical and Semiconductor Devices Group, EEE Department, Imperial College London, Exhibition Road, London SW7 2AZ, United Kingdom

[a)] Author to whom correspondence should be addressed: r.syms@imperial.ac.uk

ABSTRACT

Difficulties arise in the definition of power flow in transmission-line systems with a complex propagation constant. These were resolved by Kurokawa using quantities known as "power waves," which contain both voltage and current terms and correctly separate power flow into forward- and backward-traveling components. Similar difficulties must arise for electromagnetic metamaterials since any discrete, periodic structure leads to band-limited propagation, with a complex propagation constant both inside and outside the bands due to loss and cutoff, respectively. Here, discrete power waves are defined for magneto-inductive (MI) systems, metamaterials based on chains of magnetically coupled LC resonators. These waves are shown to satisfy the discrete power conservation equation for MI waves and are used to calculate scattering parameters for multi-port MI devices without the anomalous predictions of conventional methods. The results will allow correct evaluation of internal scattering parameters in MI systems.

I. INTRODUCTION

Scattering parameters provide tools to analyze reflection and transmission at discontinuities in electromagnetic systems or media.[1,2] However, it is well known that there may be inconsistencies when port impedances are complex or there is gain or loss.[3,4] These arise from the fact that while amplitudes are linear quantities, powers are not. Conventional definitions may then result in anomalies, such as a reflection coefficient being apparently greater than unity even for a passive load.[5] These difficulties were resolved for transmission-line systems by Kurokawa[6] and others.[7–9] For input voltages and currents v_i and i_i into a set of ports of impedance z_i, the new quantities $a_i = (v_i + z_i i_i)/\left\{2\sqrt{Re(z_i)}\right\}$ and $b_i = (v_i - z_i^* i_i)/\left\{2\sqrt{Re(z_i)}\right\}$ are introduced, where "$*$" denotes the complex conjugate. Since $\frac{1}{2}\left\{|a_i|^2 - |b_i|^2\right\} = \frac{1}{2}\mathrm{Re}(i_i v_i^*)$, forward and backward power flow may then be separately described using these "power waves" by the terms $\frac{1}{2}|a_i|^2$ and $\frac{1}{2}|b_i|^2$. This allowed a consistent definition of scattering parameters, for example, for a two-port device as $S_{11} = b_1/a_1$, $S_{12} = b_1/a_2$, $S_{21} = b_2/a_1$, and $S_{22} = b_2/a_2$.

While debate continues,[10,11] real impedance and low loss render these distinctions largely unimportant for conventional systems. However, they assume much greater significance for metamaterials, which, due to their periodic arrangement, often have complex impedance and support lossy, band-limited propagation. Here, we demonstrate the application of power waves to magneto-inductive (MI) waveguides, metamaterials based on chains of magnetically coupled LC resonators.[12,13] MI waves have been described at frequencies from RF to optical.[14–22] Passive devices have been proposed,[23,24] and applications are demonstrated in power transfer,[25–29] communications,[30–33] and sensing.[34–37] However, low-loss and in-band propagation has often been assumed.[24] Although MI systems will almost certainly be terminated using real impedance, they are becoming increasingly connected internally, and effective design then requires that intermediate scattering parameters be correctly evaluated.

The aim of this paper is to develop a power wave formulation for a periodic system supporting current waves that can be used to obtain scattering parameters at junctions between media in addition to terminations. Important differences from Kurokawa's work are introduced by the discrete nature of the system and lack of voltages at internal elements. In Sec. II, we derive the power conservation relation for MI waves. In Sec. III, we prove that discrete variants of power waves satisfy this relation and show how they may be used to find scattering parameters in MI systems. In Sec. IV,

we illustrate the process with simple examples for N-port MI devices where conventional methods break down. Conclusions are drawn in Sec. V.

II. POWER CONSERVATION IN MAGNETO-INDUCTIVE SYSTEMS

We begin by considering an infinite MI waveguide formed from magnetically coupled, lossy resonant loops, as shown in Fig. 1.

At a low frequency, the elements may be modeled as lumped circuits of inductance L (with associated resistance R) and capacitance C, coupled by mutual inductance M. For nearest-neighbor coupling, the equation relating the currents I_n in adjacent loops at angular frequency ω is

$$(R + j\omega L + 1/j\omega C)I_n + j\omega M(I_{n-1} + I_{n+1}) = 0. \quad (1)$$

The assumption of forward-going traveling wave solutions in the form $I_n = I_F \exp(-jnka)$, where I_F is the current amplitude, k is the propagation constant, and a is the element spacing, yields the well-known dispersion equation[12,13]

$$R + j\omega L + 1/j\omega C + 2j\omega M \cos(ka) = 0. \quad (2)$$

This result may be expressed alternatively in the normalized form as

$$1 - \omega_0^2/\omega^2 - j\omega_0/\omega Q + \kappa \cos(ka) = 0. \quad (3)$$

Here, $\omega_0 = 1/\sqrt{LC}$ is the resonant frequency, $Q = \omega_0 L/R$ is the quality factor, and $\kappa = 2M/L$ is the coupling coefficient. Lossless systems are band-limited to a frequency range determined by κ (which may be positive or negative), namely,

$$1/\sqrt{(1 + |\kappa|)} \le \omega/\omega_0 \le 1/\sqrt{(1 - |\kappa|)}. \quad (4)$$

Within this band, k is real, with $ka = \pi/2$ at resonance. Outside it, k abruptly becomes imaginary. It is also well known[23] that the characteristic impedance is

$$Z_0 = j\omega M \exp(-jka). \quad (5)$$

In general, Z_0 is complex. However, when k is real, we can obtain

$$\text{Re}(Z_0) = \omega M \sin(ka). \quad (6)$$

In this case, $\text{Re}(Z_0)$ reduces to $\omega_0 M$ at resonance and to zero at the band edges. Lossy systems have a complex propagation constant $k = k' - jk''$ and allow propagation out-of-band. Figure 2 shows the frequency dependence of $k'a$ and $k''a$, for example, parameters of $\kappa = 0.6, Q = 10\,000$. Here, the black dotted lines show the cutoff frequencies, highlighting the band-limited nature of propagation in low-loss systems.
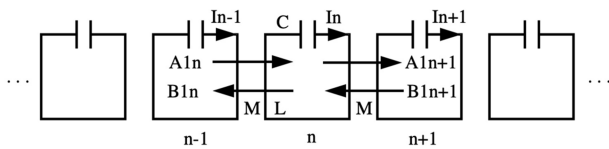

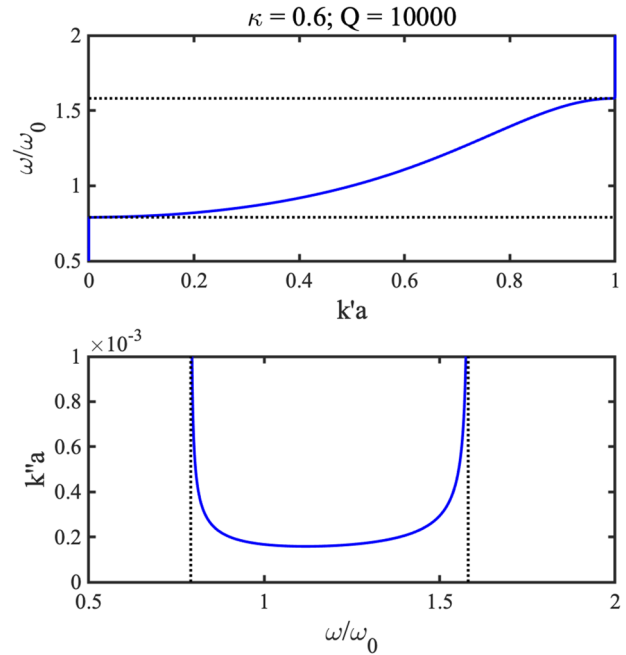FIG. 1. MI waveguide showing the direction of power flow for type 1 power waves.

FIG. 2. Frequency dependence of $k'a$ and $k''a$ for an MI waveguide with $\kappa = 0.6$, $Q = 10\,000$. Dotted lines indicate the lossless band edges.

Figure 3 shows the corresponding variation of Z_0; the wide variations in both the real and imaginary parts make broad-band impedance matching difficult.

We now consider the flow of power. Multiplying (1) by I_n^*, we get

$$(R + j\omega L + 1/j\omega C)I_n I_n^* + j\omega M(I_{n-1}I_n^* + I_n^* I_{n+1}) = 0. \quad (7)$$

Adding (7) to its own complex conjugate, dividing by 4, and rearranging, we then get

$$\frac{1}{2}RI_n I_n^* + \left(\frac{j\omega M}{4}\right)\left(I_n^* I_{n+1} - I_n I_{n+1}^*\right)$$
$$= \left(\frac{j\omega M}{4}\right)\left(I_{n-1}^* I_n - I_{n-1}I_n^*\right). \quad (8)$$
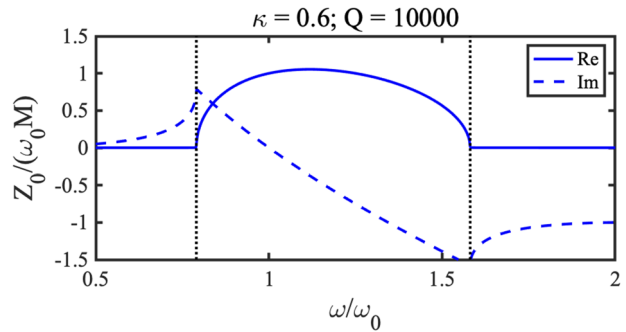

FIG. 3. Frequency dependence of Z_0 for an MI waveguide with $\kappa = 0.6$, $Q = 10\,000$.

Since the first term above is the power P_d dissipated in element n, (8) is a power conservation relation, with the second and third terms representing the powers P_{n+1} and P_n flowing into element $n+1$ from element n and into n from $n-1$, respectively. Figure 4 shows variations of P_d, P_n, and P_{n+1} with n for a very lossy MI waveguide with parameters $\kappa = 0.6$ and $Q = 10$, assuming that $L = 100$ nH, $f_0 = 1$ GHz, and $\omega/\omega_0 = 1$. Figure 4(a) shows the results obtained when there is only a forward-going wave present so that $I_n = I_F \exp(-jnka)$, with $I_F = 1$ mA. In this case, all three variations decrease exponentially with n as expected. Figure 4(b) shows results when both forward- and backward-going waves are present so that $I_n = I_F \exp(-jnka) + I_B \exp(+jnka)$, with $I_F = I_B = 1$ mA. In this case, P_d, P_n, and P_{n+1} are not (as might initially be expected) sums or differences of exponentials; there is an additional oscillation caused by beating. In both cases, we have verified that the power conservation relation (8) is satisfied.

III. DISCRETE POWER WAVES AND SCATTERING PARAMETERS

We now seek to express power flow for the discrete current waves that exist in MI systems. To do so, we introduce a discrete form of power wave. We will need two types. For lines extending to the left, we define type 1 amplitudes $A1_n$ and $B1_n$ at element n as

$$A1_n = (-j\omega M I_{n-1} + Z_0 I_n)/\left\{2\sqrt{Re(Z_0)}\right\},$$
$$B1_n = \left(-j\omega M I_{n-1} - Z_0^* I_n\right)/\left\{2\sqrt{Re(Z_0)}\right\}. \tag{9}$$

Note that these expressions contain no voltages. However, analogies with Kurokawa's a and b coefficients follow from the fact that
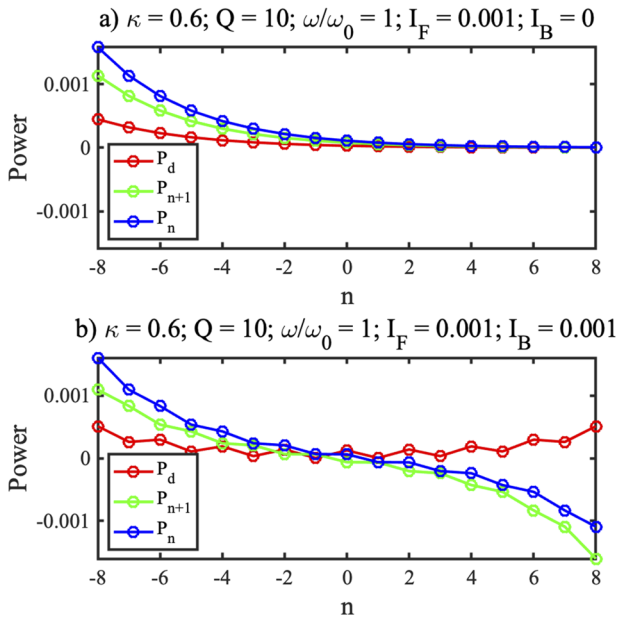

a) $\kappa = 0.6$; Q = 10; $\omega/\omega_0 = 1$; $I_F = 0.001$; $I_B = 0$

b) $\kappa = 0.6$; Q = 10; $\omega/\omega_0 = 1$; $I_F = 0.001$; $I_B = 0.001$

FIG. 4. Variation of P_d, P_n, and P_{n+1} with n for an MI waveguide with $\kappa = 0.6$, $Q = 10$, assuming $L = 100$ nH, $f_0 = 1$ GHz, $\omega/\omega_0 = 1$, and (a) $I_F = 1$ mA, $I_B = 0$ and (b) $I_F = I_B = 1$ mA.

$-j\omega M I_{n-1}$ is the voltage induced in element n by element $n-1$. Multiplying out, we get

$$|A1_n|^2 = \left\{\omega^2 M^2 I_{n-1} I_{n-1}^* + j\omega M Z_0 I_{n-1}^* I_n - j\omega M Z_0^* I_{n-1} I_n^* + Z_0 Z_0^* I_n I_n^*\right\}/\{4Re(Z_0)\},$$
$$|B1_n|^2 = \left\{\omega^2 M^2 I_{n-1} I_{n-1}^* - j\omega M Z_0^* I_{n-1}^* I_n + j\omega M Z_0 I_{n-1} I_n^* + Z_0 Z_0^* I_n I_n^*\right\}/\{4Re(Z_0)\}. \tag{10}$$

Subtracting these equations from each other and dividing by 2, we then get

$$\frac{1}{2}\left\{|A1_n|^2 - |B1_n|^2\right\} = \left(\frac{j\omega M}{4}\right)\left(I_{n-1}^* I_n - I_{n-1} I_n^*\right). \tag{11}$$

In a similar way, we can obtain

$$\frac{1}{2}\left\{|A1_{n+1}|^2 - |B1_{n+1}|^2\right\} = \left(\frac{j\omega M}{4}\right)\left(I_n^* I_{n+1} - I_n I_{n+1}^*\right). \tag{12}$$

Equations (11) and (12) may then be recognized as P_n and P_{n+1}, respectively. Substituting into (8) and re-arranging the equation so that all terms are positive, the result is

$$\frac{1}{2}R|I_n|^2 + \frac{1}{2}\left\{|A1_{n+1}|^2 + |B1_n|^2\right\} = \frac{1}{2}\left\{|A1_n|^2 + |B1_{n+1}|^2\right\}. \tag{13}$$

Equation (13) then allows the direction of the separate power flows carried by each power wave to be identified as shown in Fig. 1.

Before proceeding, we briefly consider some properties of these waves when k is real and the current consists of the sum of a forward-going wave of amplitude I_F and a backward wave of amplitude I_B so that I_n can be written as

$$I_n = I_F \exp(-jnka) + I_B \exp(+jnka). \tag{14}$$

Direct substitution shows that

$$A1_n = +\sqrt{Re(Z_0)}I_F \exp(-jnka),$$
$$B1_n = -\sqrt{Re(Z_0)}I_B \exp(+jnka). \tag{15}$$

Clearly, $A1_n$ is only dependent on I_F in this case, while $B1_n$ is only dependent on I_B. The forward and backward power flows are then

$$\frac{1}{2}|A1_n|^2 = \frac{1}{2}Re(Z_0)|I_F|^2,$$
$$\frac{1}{2}|B1_n|^2 = \frac{1}{2}Re(Z_0)|I_B|^2. \tag{16}$$

These results imply that for real k, there will be no difference between calculations based on power waves and on the moduli squared of the separate current amplitudes. However, differences are to be expected when k is complex.

We now consider the second type of discrete power wave for lines extending to the right. For consistency with Kurokawa's direction of current flow as "inward,"[6] we define type 2 amplitudes $A2_n$ and $B2_n$ at element n as

$$A2_n = (j\omega M I_{n+1} - Z_0 I_n)/\left\{2\sqrt{Re(Z_0)}\right\},$$
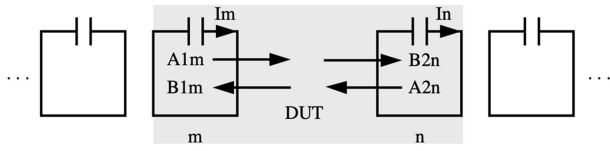$$B2_n = \left(j\omega M I_{n+1} + Z_0^* I_n\right)/\left\{2\sqrt{Re(Z_0)}\right\}. \tag{17}$$

FIG. 5. Type 1 and type 2 power waves used to find the scattering parameters of a two-port MI device.
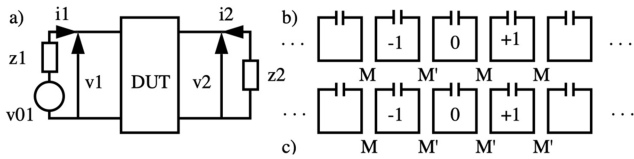

FIG. 6. (a) General two-port device and example two-port MI systems with (b) equal and (c) unequal port impedance.

Here, $j\omega MI_{n+1}$ is the voltage induced in element n by element $n + 1$. Carrying out similar manipulations, it is simple to show that

$$\frac{1}{2}R|I_n|^2 + \frac{1}{2}\left\{|A2_{n-1}|^2 + |B2_n|^2\right\} = \frac{1}{2}\left\{|A2_n|^2 + |B2_{n-1}|^2\right\}. \quad (18)$$

This power conservation relation is in a similar form to (13), but the terms are different. The two types of discrete power waves allow sources at different locations, and both are needed to compute the full set of S-parameters. For example, Fig. 5 shows a two-port MI device extending from element m to element n; here, the scattering parameters are

$$S_{11} = B1_m/A1_m, \quad S_{12} = B1_m/A2_n,$$
$$S_{21} = B2_n/A1_m, \quad S_{22} = B2_n/A2_n. \quad (19)$$

As expected, these expressions are analogous to Kurokawa's scattering parameters. Simple conclusions may be drawn immediately. For example, if k is purely imaginary, which occurs out-of-band in lossless systems, the conjugate impedance is $Z_0^* = -Z_0$. In this case, $B1_m = A1_m$ and $B2_n = A2_n$, so S_{11} and S_{22} are unity for any k.

Before presenting examples, we show how Kurokawa's scattering parameters can be found for terminated MI circuits; we term this the circuit method. Figure 6(a) shows the arrangement of a two-port device using his notation for voltages v_1 and v_2 and currents i_1 and i_2 at ports 1 and 2.

In this case, the power wave scattering parameters are

$$S_{11} = \left(v_1 - z_1^* i_1\right)/(v_1 + z_1 i_1),$$
$$S_{21} = \sqrt{\{Re(z_1)/Re(z_2)\}}\left(v_2 - z_2^* i_2\right)/(v_1 + z_1 i_1). \quad (20)$$

If v_1 is derived from a source at port 1 with voltage v_{01}, $v_1 = v_{01} - z_1 i_1$. Similarly, in the absence of a source at port 2, $v_2 = -z_2 i_2$. These results may therefore be written as

$$S_{11} = 1 - 2Re(z_1)i_1/v_{01},$$
$$S_{21} = -2\sqrt{\{Re(z_1)Re(z_2)\}}i_2/v_{01}. \quad (21)$$

These expressions allow the power wave scattering parameters to be found from a numerical solution of the circuit equations, which can yield i_1 and i_2 for a given v_{01}.

IV. EXAMPLES

We illustrate the use of the discrete power waves with examples chosen to demonstrate anomalous predictions of increasing severity using conventional methods, first involving a two-port device with equal and unequal port impedances and then a three-port device.

A. Two-port device, equal port impedances

We begin with the case shown in Fig. 6(b), namely, an MI waveguide discontinuity caused by a local variation in the mutual inductance from M to $M' = \mu M$ between two elements. We follow the approach used in Ref. 24 of finding the reflection and transmission coefficients at the junction. The governing equations are as (1) for all elements except these, where

$$(R + j\omega L + 1/j\omega C)I_{-1} + j\omega M(I_{-2} + \mu I_0) = 0,$$
$$(R + j\omega L + 1/j\omega C)I_0 + j\omega M(\mu I_{-1} + I_1) = 0. \quad (22)$$

Solutions may be found for incidence from $n = -\infty$ by assuming incident and reflected waves before the discontinuity and a transmitted wave after it so that

$$I_n = I_I \exp(-jnka) + I_R \exp(+jnka) \quad \text{for} \quad n < 0,$$
$$I_n = I_T \exp(-jnka) \quad \text{for} \quad n \geq 0. \quad (23)$$

Away from the discontinuity, these solutions satisfy Eq. (1). Substitution into (22) allows the reflection and transmission coefficients $\Gamma = I_R/I_I$ and $T = I_T/I_I$ to be found as

$$\Gamma = \frac{\left(\mu^2 - 1\right)\exp(+jka)}{\{\exp(+jka) - \mu^2 \exp(-jka)\}},$$
$$T = \frac{\mu\{\exp(+jka) - \exp(-jka)\}}{\{\exp(+jka) - \mu^2 \exp(-jka)\}}. \quad (24)$$

As expected, $\Gamma = 0$ and $T = 1$ when $\mu = 1$. For lossless systems and in-band operation, these expressions allow calculation of $|S_{11}|^2$ and $|S_{21}|^2$ as $|\Gamma|^2$ and $|T|^2$; we refer to this approach as the "modulus square" method. However, for lossy systems and/or out-of-band operation, the results can be anomalous. We illustrate this by comparison with the results obtained by (a) using the circuit method (21) with an equivalent circuit model of the system in Figs. 6(a) and 6(b) substituting (24) into expressions (9) and (17) for discrete MI power waves and then evaluating the scattering parameters using (19). In each case, the ports are effectively located at elements -1 and 0.

As a numerical example, we first assume parameters of $\kappa = 0.6$, $Q = 10\,000$, and $\mu = 1.1$, defining a weak reflector in a strongly coupled system with unfeasibly low loss. Figure 7 shows the variations with frequency of $|S_{11}|^2$ and $|S_{21}|^2$ on a dB scale obtained using the three methods. The results are qualitatively similar in each case. All three methods agree in-band, where there is high transmission. The circuit and power wave methods agree out-of-band and show high reflection in this range. However, the modulus square method predicts a reflection coefficient greater than unity here.
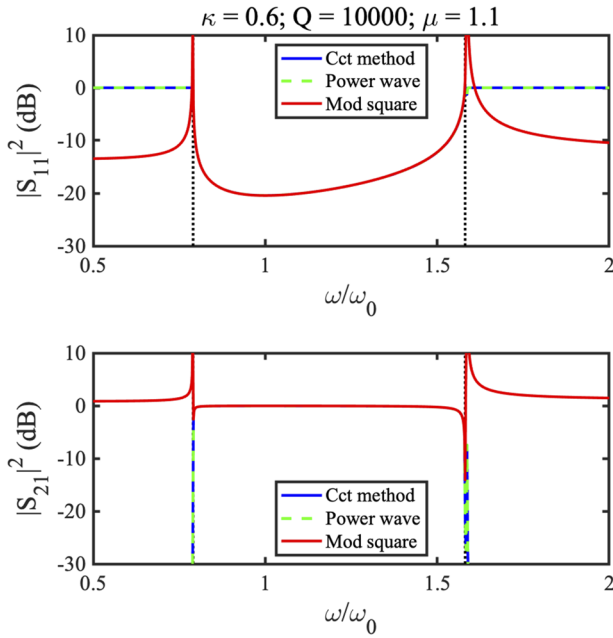
FIG. 7. Frequency dependence of $|S_{11}|^2$ and $|S_{21}|^2$ for a weak MI reflector with $\kappa = 0.6$, $Q = 10\,000$, and $\mu = 1.1$ as predicted using three different methods.
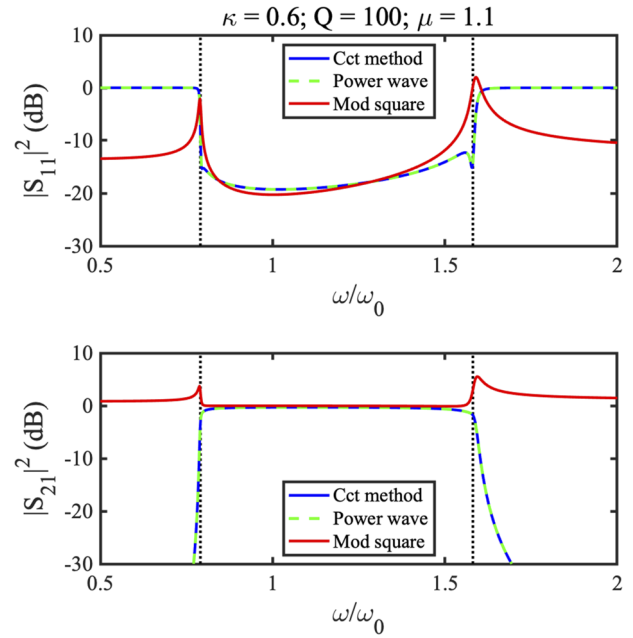

FIG. 8. Frequency dependence of $|S_{11}|^2$ for a weak MI reflector with $\kappa = 0.6$, $Q = 100$, and $\mu = 1.1$ as predicted using three different methods.

Figure 8 shows similar results for $|S_{11}|^2$ obtained with more realistic losses ($Q = 100$). The circuit and power wave calculations again agree exactly over the whole range. However, the predictions of the modulus square method are now incorrect in-band as well as out-of-band.

B. Two-port device, unequal port impedances

We now consider the case shown in Fig. 6(c), namely, a discontinuity caused by a global variation in the mutual inductance from M to $M' = \mu M$ between elements -1 and 0 and thereafter, so the system consists of two MI waveguides with different propagation constants k_1 and k_2 connected together. There are now two dispersion equations,

$$R + j\omega L + 1/j\omega C + 2j\omega M \cos(k_1 a) = 0 \quad \text{for} \quad n < -1,$$
$$R + j\omega L + 1/j\omega C + 2j\omega\mu M \cos(k_2 a) = 0 \quad \text{for} \quad n > 0. \quad (25)$$

These equations lead to characteristic impedances $Z_{01} = j\omega M \exp(-jk_1 a)$ and $Z_{02} = j\omega\mu M \exp(-jk_2 a)$ for the two lines. At the junction, the governing equations are

$$(R + j\omega L + 1/j\omega C)I_{-1} + j\omega M(I_{-2} + \mu I_0) = 0,$$
$$(R + j\omega L + 1/j\omega C)I_0 + j\omega\mu M(I_{-1} + I_1) = 0. \quad (26)$$

Assuming a solution in the form of incident, reflected, and transmitted waves, namely,

$$I_n = I_I \exp(-jnk_1 a) + I_R \exp(+jnk_1 a) \quad \text{for} \quad n < 0,$$
$$I_n = I_T \exp(-jnk_2 a) \quad \text{for} \quad n \geq 0. \quad (27)$$

The reflection and transmission coefficients may be found as

$$\Gamma = \frac{\{\mu \exp(+jk_1 a) - \exp(+jk_2 a)\}}{\{\exp(+jk_2 a) - \mu \exp(+jk_1 a)\}},$$
$$T = \frac{\{\exp(+jk_1 a) - \exp(-jk_1 a)\}}{\{\exp(+jk_2 a) - \mu \exp(+jk_1 a)\}}. \quad (28)$$

Once again, as expected, $\Gamma = 0$ and $T = 1$ when $\mu = 1$ and $k_1 = k_2$.

Scattering parameters for ports at elements -1 and 0 may again be calculated by all three methods. For example, we again assume the parameters $\kappa = 0.6$ and $Q = 100$ and take $\mu = 1.1$ so that the right-hand side line has a larger bandwidth than the left-hand side line and $|Z_{02}| > |Z_{01}|$. Figure 9 shows the frequency dependence of $|S_{11}|^2$ and $|S_{21}|^2$ calculated by all three methods on a dB scale, with the cutoff frequencies of the two lossless bands marked using black dotted and dotted-dashed lines. Once again, the circuit and power wave methods agree exactly. The modulus square method agrees reasonably inside the smaller band, when k_1 and k_2 are both approximately real. However, it predicts unphysical results when either or both of k_1 and k_2 have significant imaginary parts.

C. Three-port device, equal port impedances

We now consider the three-port splitter shown in Fig. 10 and formed from three MI waveguides with identical characteristics. These support currents $I_{i,n}$, where $i = 1, 2, 3$. Line 1 extends from $n = -\infty$ to $n = -1$, and lines 2 and 3 extend from $n = 1$ to $n = +\infty$. The three lines are coupled together at element 0, which has mutual inductance $M_i = \mu_i M$ to line i. Elsewhere, the three lines have
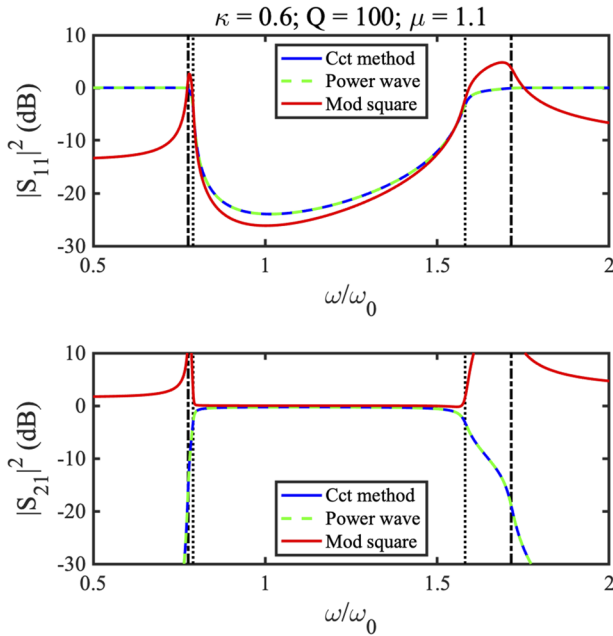
FIG. 9. Frequency dependence of $|S_{11}|^2$ and $|S_{21}|^2$ for a junction between two MI waveguides with $\kappa = 0.6$, $Q = 100$, and $\mu = 1.1$ as predicted using three different methods. Black dashed and dotted-dashed lines show the lossless band edges.

parameters R, L, C, and M, and the dispersion equation is analogous to (1).

The equations that must be solved at the junction are

$$
\begin{aligned}
(R + j\omega L + 1/j\omega C)I_{1,-1} + j\omega M(I_{1,-2} + \mu_1 I_0) &= 0, \\
(R + j\omega L + 1/j\omega C)I_0 + j\omega M(\mu_1 I_{1,-1} + \mu_2 I_{2,1} + \mu_3 I_{3,1}) &= 0, \\
(R + j\omega L + 1/j\omega C)I_{2,1} + j\omega M(I_{2,2} + \mu_2 I_0) &= 0, \\
(R + j\omega L + 1/j\omega C)I_{3,1} + j\omega M(I_{3,2} + \mu_3 I_0) &= 0.
\end{aligned}
\tag{29}
$$

Here, I_0 is the current at the connecting loop, a separate unknown. For incidence from line 1, solutions are assumed as

$$
\begin{aligned}
I_{1,n} &= I_I \exp(-jnka) + I_R \exp(+jnka) \quad \text{for} \quad n < 0, \\
I_{2n} &= I_{T2} \exp(-jnka) \text{for} \quad n > 0, \\
I_{3n} &= I_{T3} \exp(-jnka) \text{for} \quad n > 0.
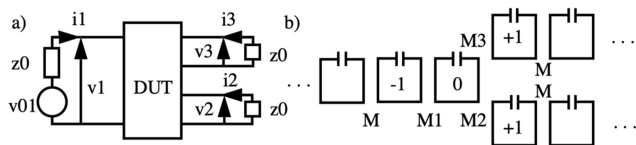\end{aligned}
\tag{30}
$$

FIG. 10. Three-port MI splitter: (a) port definition and (b) physical arrangement.

Substituting and making use of the dispersion equation, solutions can be obtained as[24]

$$
\begin{aligned}
\Gamma &= \frac{I_R}{I_I} = \frac{(1 - \mu_1^2)\exp(+jka) - (\mu_2^2 + \mu_3^2 - 1)\exp(-jka)}{(\mu_1^2 + \mu_2^2 + \mu_3^2 - 1)\exp(-jka) - \exp(+jka)}, \\
T_2 &= \frac{I_{T2}}{I_I} = \frac{\mu_1\mu_2\{\exp(-jka) - \exp(+jka)\}}{(\mu_1^2 + \mu_2^2 + \mu_3^2 - 1)\exp(-jka) - \exp(+jka)}, \\
T_3 &= \frac{I_{T3}}{I_I} = \frac{\mu_1\mu_3\{\exp(-jka) - \exp(+jka)\}}{(\mu_1^2 + \mu_2^2 + \mu_3^2 - 1)\exp(-jka) - \exp(+jka)}.
\end{aligned}
\tag{31}
$$

Here, we focus on the case when $\mu_1 = 1$ and $\mu_2^2 + \mu_3^2 = 1$ and (31) reduces to $\Gamma = 0$, $T_2 = \mu_2$, and $T_3 = \mu_3$, implying that the splitter is matched and has a constant splitting ratio. Using the circuit method, equations are solved for the four loops, assuming a voltage source with output impedance Z_0 at port 1 and terminations at ports 2 and 3, as shown in Fig. 10(a). Using discrete power waves, A and B coefficients are found for each line in turn. Figure 11 shows the frequency dependence on a dB scale of $|S_{11}|^2$ and $|S_{21}|^2$ thus obtained for a splitter with parameters $\kappa = 0.6$, $Q = 100$, $\mu_1 = 1$, and $\mu_2 = \mu_3 = 1/\sqrt{2}$, so the device is a 3dB splitter. As usual, the black dotted lines show the lossless band edges. The predictions of the modulus square method are entirely incorrect for $|S_{11}|^2$ since this trace is absent. Although the predictions for $|S_{21}|^2$ (and $|S_{31}|^2$, since this is identical) are qualitatively correct in-band, only the circuit and power wave methods show the expected band-limited performance.

These results highlight the need to obtain realistic estimates of power flow when there is loss and/or when propagation is out-of-band. For terminated ports, the circuit method of Eq. (21) gives
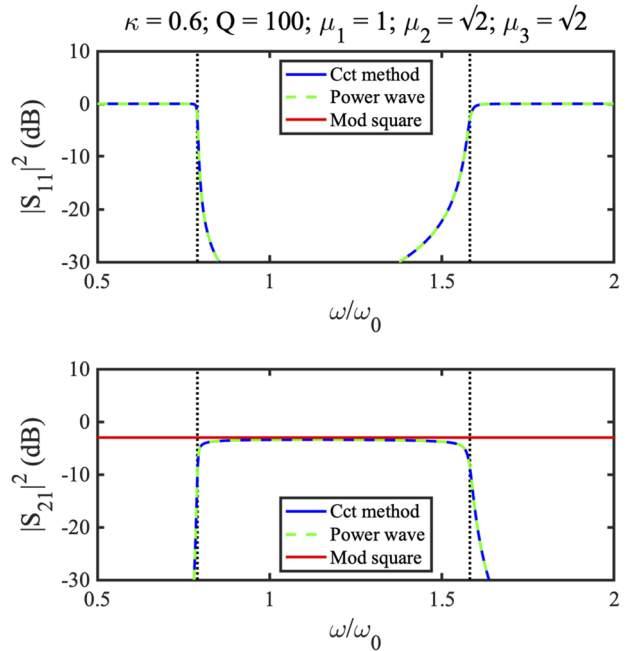

FIG. 11. Frequency dependence of $|S_{11}|^2$ and $|S_{21}|^2$ for a 3dB MI splitter with parameters $\kappa = 0.6$, $Q = 100$, $\mu_1 = 1$, and $\mu_2 = \mu_3 = 1/\sqrt{2}$ as predicted using three different methods. Black dashed lines show the lossless band edges.

numerical results that are universally equivalent to those obtained using Kurokawa's method.[6] However, the discrete power wave method also allows scattering parameters to be found when there is no immediately adjacent port, for example, at junctions between semi-infinite media. As we have shown numerically, this allows direct exploitation of the solutions of boundary matching problems. Although these are not presented here due to their length, we have also used known results for Γ and T to construct complete analytic expressions for the S-parameters themselves.

V. CONCLUSIONS

A discrete formulation of power waves has been developed for magneto-inductive waveguides. These waves are analogous to the continuous power waves introduced by Kurokawa for transmission-line systems, satisfy the power conservation relation, and avoid the physical anomalies seen in scattering parameters found using modulus square methods for passive MI systems. They are applicable to a system supporting pure current waves and allow determination of intermediate scattering parameters, for example, at junctions between semi-infinite media.

The importance of the power wave approach has been demonstrated using examples involving multi-port MI devices, which show how analytic solutions can be correctly converted to scattering parameters. Consequently, this approach should assist in designing systems that involve connected MI devices (for example, containing splitting or filtering components as well as simple propagation pathways). Since an analogous power conservation relation may be constructed for MI waves in 2D, assuming mutual inductances M_x and M_y in the two perpendicular directions, it may be useful for calculating power flow in devices based on metasurfaces. Finally, it is likely to be relevant to other periodic metamaterials, such as electro-inductive waveguides,[38] for which discrete power waves may also be constructed.

DATA AVAILABILITY

The data that support the findings of this study are available within the article.

REFERENCES

[1] E. W. Matthews, "The use of scattering matrices in microwave circuits," IRE Trans. Microwave Theory Tech. **3**, 21–26 (1955).

[2] H. Carlin, "The scattering matrix in network theory," IRE Trans. Circuit Theory **3**, 88–97 (1956).

[3] D. Youla, "On scattering matrices normalized to complex port numbers," Proc. IRE **49**, 1221 (1961).

[4] P. Penfield, "Noise in negative resistance amplifiers," IRE Trans. Circuit Theory **7**, 166–170 (1960).

[5] S. C. Dutta Roy, "Some little-known facts about transmission lines and some new results," IEEE Trans. Educ. **53**, 556–561 (2010).

[6] K. Kurokawa, "Power waves and the scattering matrix," IEEE Trans. Microwave Theory Tech. **13**, 194–202 (1965).

[7] G. E. Stannard, "Calculation of power on a transmission line," Proc. IEEE **55**, 132 (1967).

[8] R. J. Vernon and S. R. Seshadri, "Reflection coefficient and reflected power on a lossy transmission line," Proc. IEEE **57**, 101–102 (1969).

[9] J. Rahola, "Power waves and conjugate matching," IEEE Trans. Circuits Syst., II **55**, 92–96 (2008).

[10] S. Liorente-Romano, A. Garcia-Lampérez, T. K. Sarkar, and M. Salazar-Palma, "An exposition on the choice of proper S parameters in characterizing devices including transmission lines with complex impedances and a general methodology for calculating them," IEEE Antennas Propag. Mag. **55**, 94–112 (2013).

[11] D. Williams, "Traveling waves and power waves: Building a solid foundation for microwave circuit theory," IEEE Microwave Mag. **14**, 38 (2013).

[12] E. Shamonina, V. A. Kalinin, K. H. Ringhofer, and L. Solymar, "Magneto-inductive waveguide," Electron. Lett. **38**, 371–373 (2002).

[13] M. C. K. Wiltshire, E. Shamonina, I. R. Young, and L. Solymar, "Dispersion characteristics of magneto-inductive waves: Comparison between theory and experiment," Electron. Lett. **39**, 215–217 (2003).

[14] M. J. Freire, R. Marqués, F. Medina, M. A. G. Laso, and F. Martín, "Planar magneto-inductive wave transducers: Theory and applications," Appl. Phys. Lett. **85**, 4439–4441 (2004).

[15] M. C. K. Wiltshire, E. Shamonina, I. R. Young, and L. Solymar, "Experimental and theoretical study of magneto-inductive waves supported by one-dimensional arrays of 'swiss rolls,'" J. Appl. Phys. **95**, 4488–4493 (2004).

[16] G. Dolling, M. Wegener, A. Schädle, S. Burger, and S. Linden, "Observation of magnetization waves in negative-index photonic metamaterials," Appl. Phys. Lett. **89**, 231118 (2006).

[17] I. V. Shadrivov, A. N. Reznik, and Y. S. Kivshar, "Magnetoinductive waves in arrays of split-ring resonators," Physica B **394**, 180–183 (2007).

[18] N. Liu, S. Kaiser, and H. Giessen, "Magnetoinductive and electroinductive coupling in plasmonic metamaterial molecules," Adv. Mater. **20**, 4521–4525 (2008).

[19] J. D. Baena, L. Jelinek, R. Marques, and M. Silveirinha, "Unified homogenization theory for magnetoinductive and electroinductive waves in split-ring metamaterials," Phys. Rev. A **78**, 013842 (2008).

[20] H. Liu, Y. M. Liu, S. M. Wang, S. N. Zhu, and X. Zhang, "Coupled magnetic plasmons in metamaterials," Phys. Status Solidi B **246**, 1397–1406 (2009).

[21] S. Campione, F. Mesa, and F.Capolino, "Magneto-inductive waves and complex modes in two-dimensional periodic arrays of split ring resonators," IEEE Trans. Antennas Propag. **61**, 3554–3563 (2013).

[22] C. J. Stevens, Y. Li, and C. W. T. Chen, "Forward magneto-inductive wave propagation in planar magnetically coupled capacitor grids," J. Electromagn. Waves Appl. **29**, 753–762 (2015).

[23] E. Shamonina and L. Solymar, "Magneto-inductive waves supported by metamaterial elements: Components for a one-dimensional waveguide," J. Phys. D: Appl. Phys. **37**, 362–367 (2004).

[24] R. R. A. Syms, E. Shamonina, and L. Solymar, "Magneto-inductive waveguide devices," IEE Proc.-Microwaves, Antennas Propag. **153**, 111–121 (2006).

[25] A. Kurs, A. Karalis, R. Moffatt, J. D. Joannopoulos, P. Fisher, and M. Soljacic, "Wireless power transfer via strongly coupled magnetic resonances," Science **317**(5834), 83–86 (2007).

[26] W. Zhong, C. K. Lee, and S. Y. R. Hui, "General analysis on the use of Tesla's resonators in domino forms for wireless power transfer," IRE Trans. Ind. Electron. **60**, 261–270 (2013).

[27] B. Wang, W. Yerazunis, and K. H. Teo, "Wireless power transfer: Metamaterials and array of coupled resonators," Proc. IEEE **101**, 1359–1368 (2013).

[28] C. J. Stevens, "Magneto-inductive waves and wireless power transfer," IEEE Trans. Power Electron. **30**, 6182–6190 (2014).

[29] F. S. Sandoval, S. M. T. Delgado, A. Moazenzadeh, and U. Wallrabe, "A 2D magneto-inductive wave device for freer wireless power transmission," IEEE Trans. Power Electron. **34**, 10433–10445 (2019).

[30] C. J. Stevens, C. W. T. Chan, K. Stamatis, and D. J. Edwards, "Magnetic metamaterials as 1-D data transfer channels: An application for magneto-inductive waves," IEEE Trans. Microwave Theory Tech. **58**, 1248–1256 (2010).

[31] C. W. T. Chan and C. J. Stevens, "Two-dimensional magneto-inductive wave data structures," in *Proceedings of the EUCAP Conference* (IEEE, 2011), Vol. 11-15, pp. 1071–1075.

[32] B. Gulbahar and O. B. Akan, "A communication theoretical modeling and analysis of underwater magneto-inductive wireless channels," IEEE Trans. Wireless Commun. **11**, 3326–3334 (2012).

[33]Z. Sun and I. F. Akyildiz, "Magnetic induction communications for wireless underground sensor networks," IEEE Trans. Antennas Propag. **58**, 2426–2435 (2010).

[34]Y. Chen, S. Munukutia, P. Pasupathy, D. P. Neikirk, and S. L. Wood, "Magneto-inductive waveguide as a passive wireless sensor network for structural health monitoring," Proc. SPIE **7647**, 764749 (2010).

[35]T. Floume, "Magneto-inductive conductivity sensor," Metamaterials **5**, 206–217 (2011).

[36]C. J. Stevens, J. Yan, and E. Shamonina, "A meta-material position sensor based on magneto-inductive waves," in 13th International Congress on Metamaterials, Rom, Italy, 16–21 2019.

[37]R. R. A. Syms, I. R. Young, M. M. Ahmad, and M. Rea, "Magnetic resonance imaging with linear magneto-inductive waveguides," J. Appl. Phys. **112**, 114911 (2012).

[38]M. Beruete, F. Falcone, M. J. Freire, R. Marqués, and J. D. Baena, "Electroinductive waves in chains of complementary metamaterial elements," Appl. Phys. Lett. **88**, 083503 (2006).